Memoirs of the Faculty of Engineering, Kyushu University, Vol.66, No.3, September 2006

A New Approach to Airborne Mine Detection Scheme Using a Magnetic Gradiometer

by

Koki FUJITA*, Ken-ichiro ONAKA** and Norihiro GOTO***

(Received July 28, 2006)

Abstract

This paper proposes a new approach to improving the 2-D mine detection scheme utilizing an airborne system such as a blimp. At Kyushu University, a mine detection system using a blimp has been developed[1)]. A magnetic gradiometer is appropriate for land mines including ferromagnetic material. Effective observation signals such as Amplitude Analytic Signal are applicable to the detection of any anomalies in mine field. However, a sensor is exposed to electromagnetic noises caused by other metallic devices onboard, and its performance is very sensitive to the location of a sensor on the blimp. Therefore, this study proposes a technique to obtain the planar positions of land mines from the original data with observation noises. In the proposed scheme, the magnitude of dipole magnetic induction is estimated assuming that dipoles are buried in all the grid points over which magnetic gradient data are obtained. The effectiveness of the proposed method is demonstrated through numerical simulations and indoor experiments.

Keywords: Airborne mine detection system, Magnetic gradiometer, Dipole magnetic field, Noise filtering, LS method

1. Introduction

Land mines left in old battle fields such as South-East Asia and Middle East are hampering the reconstruction and development of the countries in the regions. Today, most of the land mines are removed manually by civilian, thereby constantly increasing the number of victims. Statistics report that twenty five thousand people get injured in nearly ninety countries, every year.

* Research Associate, Department of Aeronautics and Astronautics
** Graduate Student, Department of Aeronautics and Astronautics (currently, All Nippon Airways Co., Ltd.)
*** Professor, Department of Aeronautics and Astronautics

At Kyushu University, a mine detection system using a blimp has been developed[1)] and researches of concern mainly have focused on the identification of the blimp's aerodynamics and on the control theories that are robust to the envelope's flexibilities and external disturbances such as wind gust.

On the other hand, effective methods to detect land mines using a magnetic gradiometer also have been developed. Because the sensor is housed onboard the blimp in flight, observed data are disturbed by other onboard equipments such as inertial navigation system, altimeter, radio transmitter, and so on. Therefore, this study proposes a mine detection method which has robustness to noisy environment.

2. Mine Detection System Using a Blimp

2.1 Sky Probe-J

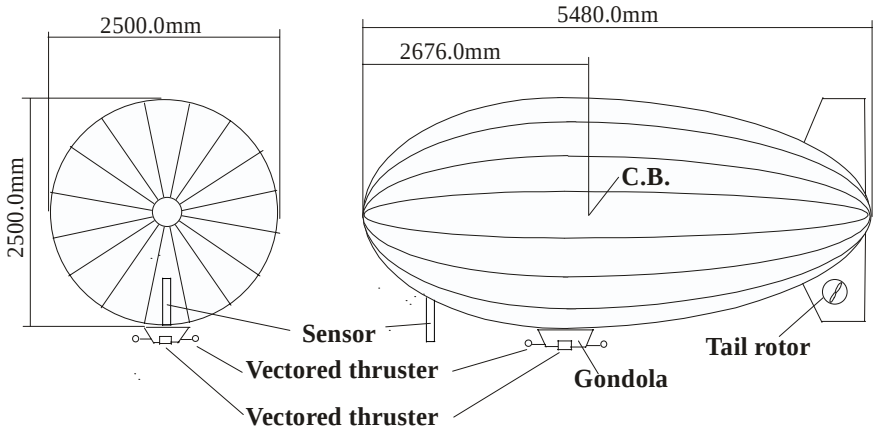

Fig.1 Sky Probe-J.

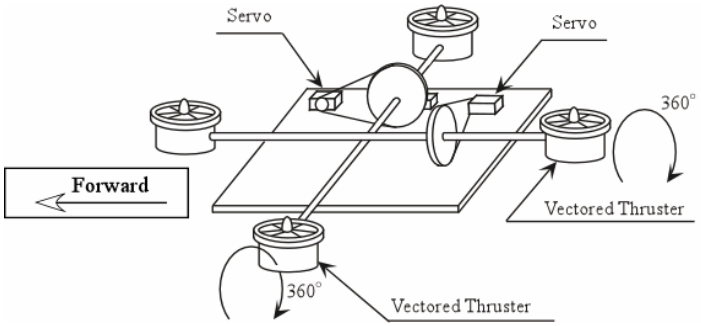

Fig.2 Propulsion System of Sky Probe-J.

Figures 1 and **2** show the blimp named Sky Probe-J which belongs to Kyushu Univ., and its propulsion system attached to the gondola. The specifications of the blimp are shown in **Table 1**. As shown in **Fig. 1**, the sensor (magnetic gradiometer) is loaded on forward part of the blimp's envelope.

Table 1 Dimensional data for Sky Probe-J.

Hull	Envelope shape along the axis of symmetry: $\frac{x^2}{a^2}+\frac{y^2}{b^2}=1 \ (x<0)$ $\frac{x^2}{2a^2}+\frac{y^2}{b^2}=1 \ (x\geq 0)$ $(a=2.27\ \mathrm{m}, b=1.25\ \mathrm{m})$ Length: 54776.6 mm Maximum diameter: 2500.00 mm Volume: 18.0 m^3
Propulsion	4 vectored thrusters: 400 gf for each 2 tail rotors: 100 gf for each
Fins	Cross-wing: NACA0008

2.2 Land mines in this study

Most of land mines can be divided into two types depending on the objectives of damage; Anti-Personnel Mine and Anti-Tank Mine. While many land mines come to be made of plastic materials, most of anti-tank mines are still made of metallic ones, which can be detected by magnetic sensors. Therefore, we apply a strategy to remove all the land mines step by step in a mine field as follows:

STEP1: A mine detection scheme aiming at anti-tank mines.
STEP2: Another mine detection scheme aiming at anti-personnel mines.

In this study, in order to detect land mines made of metallic materials such as anti-tank mines, effective methods using a magnetic gradiometer are proposed.

3. Dipole Magnetic Field Estimation Using Magnetic Gradiometer

3.1 Dipole magnetic field

The magnetic induction or simply *the magnetic field* of a dipole observed at points other than the dipole itself is shown as follows[2].

$$\mathbf{B}=C_m\frac{m_d}{r^3}\left[3(\hat{\mathbf{m}}\cdot\hat{\mathbf{r}})\hat{\mathbf{r}}-\hat{\mathbf{m}}\right], \qquad \mathrm{r}\neq 0, \tag{1}$$

where, $\hat{\mathbf{m}}$ is the dipole moment which has the magnitude of m_d [Am^2]. $\hat{\mathbf{r}}$ is the vector from the dipole's source to the observation point, which has the distance of r [m]. C_m is a proportionality constant, which is reduced to $\mu_0/(4\pi)=10^{-7}$[henry$\cdot\mathrm{m}^{-1}$] in SI units. m_d is obtained from the magnitude of the magnetization of the magnetic source multiplied by its volume.

Eq. (1) is expressed for each component of 3-D Cartesian coordinates as,

$$B_x = K\frac{3Dx - r^2 l}{r^5}, \tag{2a}$$

$$B_y = K\frac{3Dy - r^2 m}{r^5}, \tag{2b}$$

$$B_z = K\frac{3Dz - r^2 n}{r^5}, \tag{2c}$$

where, $K\,(=C_m m_d)$ is a proportionality constant, and x, y, and z are the elements of the vector $\hat{\mathbf{r}}$ in the Cartesian coordinates, that is, $r=\sqrt{x^2+y^2+z^2}$. l, m, n, and D are the parameters concerned with the direction of the magnetization of the dipole, and each can be denoted using inclination angle, α and declination angle, β (**Fig.3**) as follows:

$$l = \cos\alpha \cdot \cos\beta\,, \tag{3a}$$

$$m = \cos\alpha \cdot \sin\beta\,, \tag{3b}$$

$$n = \sin\alpha\,, \tag{3c}$$

$$D = lx + my + nz\,. \tag{3d}$$

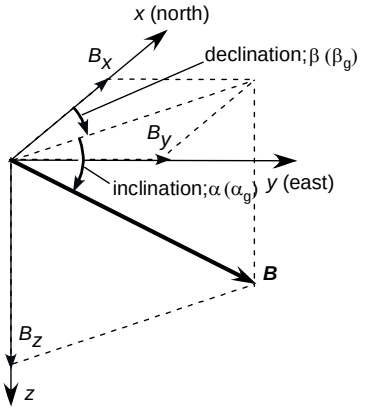

Fig.3 Inclination and declination angles with the magnetization of a dipole.

3.2 Observation signal to detect magnetic anomalies

To detect anomalies in the magnetic field, one of the effective signals to be observed is, so called, AAS (Amplitude Analytic Signal) such that

$$A(x,y,z) = \sqrt{\left(\frac{\partial T}{\partial x}\right)^2 + \left(\frac{\partial T}{\partial y}\right)^2 + \left(\frac{\partial T}{\partial z}\right)^2}\,. \tag{4}$$

T implies the magnitude of the anomaly in the magnetic field, which is derived as follows:

$$T = LB_x + MB_y + NB_z\,, \tag{5}$$

where, L, M and N relate to the direction of geomagnetic field, and are defined with respect to the inclination and the declination angles, α_g and β_g by

$$L = \cos\alpha_g \cdot \cos\beta_g\,, \tag{6a}$$

$$M = \cos\alpha_g \cdot \sin\beta_g , \tag{6b}$$

$$N = \sin\alpha_g . \tag{6c}$$

The AAS is an effective signal because it is not influenced by the magnetization direction of the anomaly source which is generally unknown[3]. On the other hand, considering the experimental condition with a magnetic gradiometer which is vertically hung on the blimp, the following signal is more practical:

$$A_{grad}(x, y, z) = \sqrt{\left(\frac{\partial B_x}{\partial z}\right)^2 + \left(\frac{\partial B_y}{\partial z}\right)^2 + \left(\frac{\partial B_z}{\partial z}\right)^2} \tag{7}$$

Because the magnetic gradiometer is fixed on the blimp in such a way that the two endpoint-sensors may align with the z-axis of the inertial coordinate system, the partial derivatives of B_x, B_y, and B_z with respect to z are straightforwardly obtained from the sensor without any coordinate transformations.

According to Eqs. (2a) to (2c), Eq. (7) is reduced to

$$A_{grad}(x, y, z, \alpha, \beta) = \frac{3K}{r^5}\sqrt{\left(\frac{5z^2}{r^2}+1\right)D^2 - 4Dnz + n^2r^2 + z^2} . \tag{8}$$

We should note here that $r \propto (x, y, z)$, $n \propto \alpha$, and $D \propto (x, y, z, \alpha, \beta)$, which means that A_{grad} is a nonlinear function of the observation point from the dipole magnetic source, (x, y, z), as well as the magnetization direction of each dipole, (α, β). If artificial magnetic sources such as land mines are buried at the same depth, z can be almost constant such that $z \cong z_c$. On the other hand, after x and y are transformed into non-dimensional variables; i.e. $x' = x / z$, $y' = y / z$, Eq. (8) is reduced to

$$A_{grad}(x', y', \alpha, \beta) = \frac{3K}{r'^5}\sqrt{\left(\frac{5}{r'^2}+1\right)D'^2 - 4D'n + n^2r'^2 + 1}, \tag{9}$$

where $r' = \sqrt{x'^2 + y'^2 + 1}$ and $D' = lx' + my' + n$.

Figure 4 depicts the value of A_{grad} with respect to x' and y' assuming that $\alpha = \beta = 0\,[\text{rad}]$. In **Fig.5** are shown the effects of α and β on A_{grad} for various positions around a magnetic source. For all the cases, the proportionality constant, K is fixed at 1.0 [Tm^3]. As shown in the figures, the parameters concerned with the direction of the magnetization, α and β, have little effect on A_{grad} except at the point just over the magnetic source, which is a favorable property for detecting the position of a magnetic source in the *x*-*y* plane. Thus, in the following sections the estimation scheme will be proposed under the assumption that

$$A_{grad}(x, y, z, \alpha, \beta) \cong kA_{grad}(x', y', \alpha_c, \beta_c) , \tag{10}$$

where α_c and β_c are fixed for all the magnetic sources, and k is a constant depending on each magnetic source.

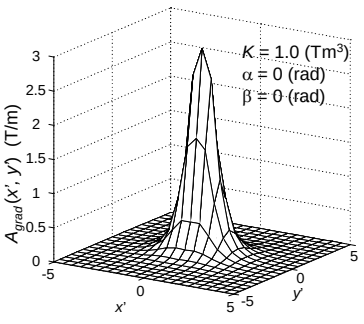

Fig.4 The effects of *x'* and *y'* on the observed signal, A_{grad}.

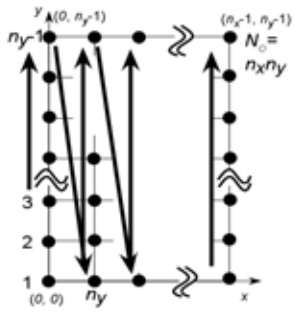

Fig.6 Observation grid points on a mine field.

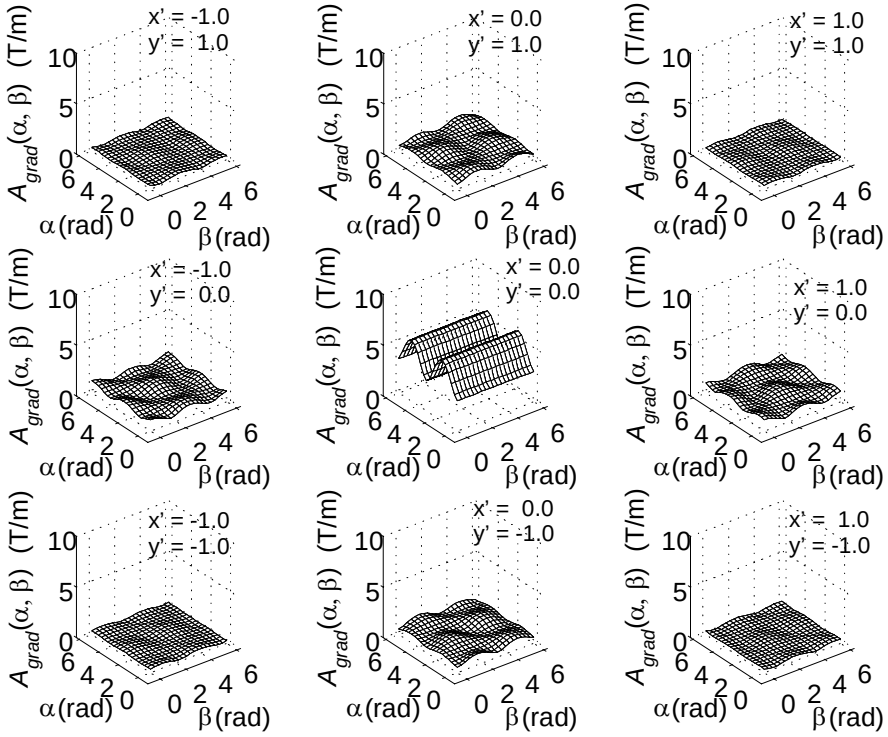

Fig.5 The effects of α and β on A_{grad}.

3.3 An estimation method to detect planar position of magnetic anomaly

If the observation signal, A_{grad} is obtained over the *j*-th grid point ($j = 1,2,3,\cdots,N_o$) on the ground as shown in **Fig. 6**, the relationship between $A_{grad}(j)$ and a variable concerned with the magnitude of the magnetic induction of a virtual dipole buried at the *i*-th grid point, $K_s(i)$ ($i = 1,2,3,\cdots,N_s$) is denoted as follows:

$$A_{grad}(j) = C_{ij} K_s(i) + N(j), \tag{11}$$

$$C_{ij} = \frac{3}{r_{ij}'^{5}} \sqrt{\left(\frac{5}{r_{ij}'^{2}} + 1 \right) D_{ij}'^{2} - 4 D_{ij}' n_i + n_i^{2} r_{ij}'^{2} + 1}\,, \tag{12}$$

$$r_{ij}' = \sqrt{(x_i' - x_j')^2 + (y_i' - y_j')^2 + 1}\,, \tag{13}$$

$$D_{ij}' = l_i(\alpha_c, \beta_c) \cdot (x_i' - x_j') + m_i(\alpha_c, \beta_c) \cdot (y_i' - y_j') + n_i(\alpha_c, \beta_c)\,, \tag{14}$$

where, $N(j)$ is observation noise at the *j*-th grid point, (x_i', y_i') and (x_j', y_j') are the non-dimensional 2-D position of the *i*-th and *j*-th grid points, respectively. Considering the assumption that A_{grad} should approximately depend on x' and y', $K_s(i)$ is defined by

$$K_s(i) = k(i)K(i). \tag{15}$$

$K(i)$ is the proportionality constant with respect to the dipole magnetic induction, and $k(i)$ is the constant depending on the magnetization direction of each dipole magnetic source.

Alternatively, the above equations are expressed in a matrix form such as,

$$\mathbf{A_{grad}} = \mathbf{C}\mathbf{K_s} + \mathbf{N}\,, \tag{16}$$

where, $\mathbf{A_{grad}} \in \mathbf{R}^{N_o \times 1}$, $\mathbf{K_s} \in \mathbf{R}^{N_s \times 1}$, $\mathbf{N} \in \mathbf{R}^{N_s \times 1}$ and $\mathbf{C} \in \mathbf{R}^{N_o \times N_s}$.

As previously mentioned, the data obtained from an onboard magnetic gradiometer are disturbed by noises, **N**, from other devices on the blimp. Therefore, Eq. (16) is feasible for an internal expression of the observed signal over a dipole magnetic field. From Eq. (16), $\mathbf{K_s}$, which is equivalent to the magnitude of the magnetic induction of the dipole buried at the *i*-th $(i = 1,2,3,\cdots, N_s)$ grid point is estimated as follows:

$$\hat{\mathbf{K}}_\mathbf{s} = \mathbf{C}^{*}\mathbf{A_{grad}}\,, \tag{17}$$

where, $\mathbf{C}^{*}$ is the pseudo inverse matrix, $\mathbf{C}^{*} = (\mathbf{C}^T\mathbf{C})^{-1}\mathbf{C}^T$.

$\hat{\mathbf{K}}_\mathbf{s}$ is the solution by the Least Squares (LS) method, and if the depth of each dipole magnetic source is nearly constant ($z \cong z_c$), then their planar positions have now been identified out of the data with noises. The above estimation algorithm is applied to the case where, N_s is constrained to be less than N_o ($N_s \le N_o$).

4. Numerical Simulations and Indoor Experiments

4.1 Numerical simulations for the case without observation noises

The effectiveness of the proposed method to detect magnetic sources is now demonstrated through numerical simulations. **Table 2** shows the parameter setting for the simulations CASE1. According to **Table 2**, the magnitude of the dipole moment as anomaly sources can be calculated as

$$m_d = 1000 \times \pi \times (0.2)^2 \times 0.1 = 12.6 \quad [\mathrm{Am}^2] \tag{18}$$

For the above simulation model, 2-D distribution of B_x, B_y, B_z and B in *x'*-*y'* field are shown in **Figs. 7** to **10**. The ideal distributions of the observation signals, AAS and A_{grad} for the dipole magnetic field are shown in **Fig.11** and **Fig.12**.

Table 2 Simulation Model (CASE1).

Positions of Magnetic Sources	(x, y, z) = (21.0 14.0 -1.0), (15.0 35.0 -2.0), (30.0 25.0 -0.5), (19.0 12.0 -1.0)
Amplitude of Uniform Magnetization*1	1000 [A/m]
Size of Magnetic Sources*1	A right cylinder with 0.2 m diameter and 0.1m height
Inclination and Declination Angles of Geomagnetic Field	$a_g = 47^\circ 38^{''}$, $\beta_g = 6^\circ 35^{''}$
Size of an Observation Field	40 [m] × 40 [m]
Height of Observation	$z_o = 1.0$ [m]
Number of Grid Points for Observation*2	$N_o = 40 \times 40$ [points]
Number of Grid Points for Magnetic Source Estimation*2	$N_s = 40 \times 40$ [points]

*1 for all the anomalies, *2 uniformly distributed in the observation field.

According to the both observation signals, the positions of the anomaly sources can be precisely estimated from AAS or A_{grad}, if any noises are not included in the original observation data. Next, **Fig.13** shows the 2-D distribution of K_s estimated by using Eq. (17). For all these results, the inclination and the declination angles of the magnetization of the anomaly sources were assumed to be $\alpha = 0.0$ [rad] and $\beta = 0.0$ [rad]. As shown in **Fig.13**, the estimated values of K_s clearly show the positions of the anomaly sources as well as the original observation data do.

4.2 Numerical simulations for the case with observation noises

Numerical simulations considering observation noises are then conducted. The simulation model in this case, CASE2 is described in **Table 3**. The inclination and the declination angles of the magnetization for all the anomaly sources are assumed to be $\alpha = 0.0$ [rad] and $\beta = 0.0$ [rad], which are also used to estimate K_s from observation data. **Figure 14** shows the 2-D distribution of the observation signal, $A_{grad}(x', y')$ for this case. As seen in the figure, the anomaly position, (6.0, 4.0, -0.5), in which the magnetic source (a land mine) is assumed to be shallowly buried, is precisely detected by the signal. However, the other two anomaly sources are hard to be detected only by the magnitudes of the signals.

On the other hand, from the 2-D distribution of the estimated K_s as seen in **Fig.15**, noises are effectively removed and two anomaly sources buried at (6.0, 4.0, -0.5) and (3.0, 2.0, -1.0) are detected more clearly than from $A_{grad}(x', y')$. Furthermore, all the anomaly sources are detected more precisely in limited regions.

The robustness to the estimation error of the unobserved land mine's magnetization direction is also demonstrated as follows: Assuming that the inclination and declination angles of the magnetization for all the anomaly sources are $\alpha = \pi / 6.0$ [rad] and $\beta = \pi / 6.0$ [rad], the 2-D distribution of A_{grad} can be calculated as shown in **Fig.16**. In this case, the anomaly sources are sufficiently well detected through the observation data because the magnitudes of the observation signals at each magnetic source are greater than those in the previous case.

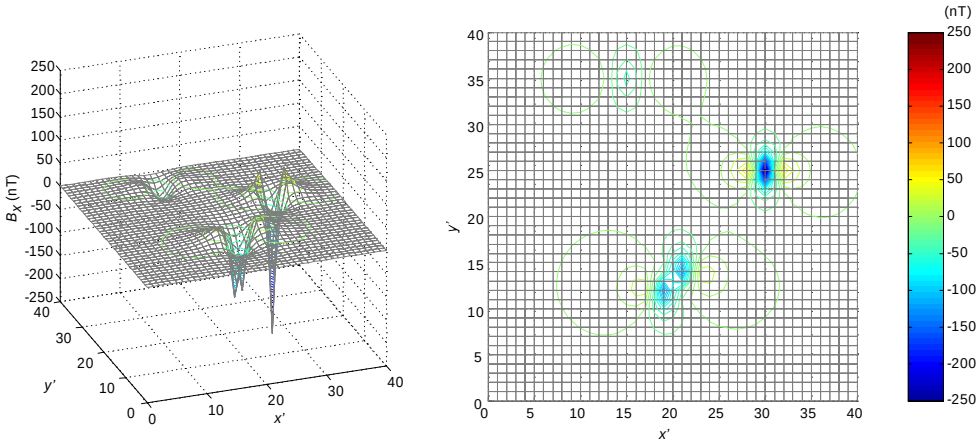

Fig.7 2-D distribution of B_x (CASE1).

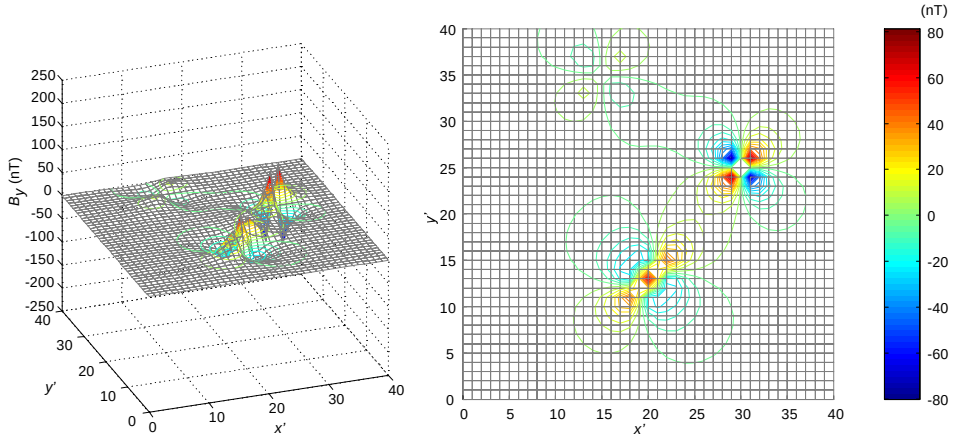

Fig.8 2-D distribution of B_y (CASE1).

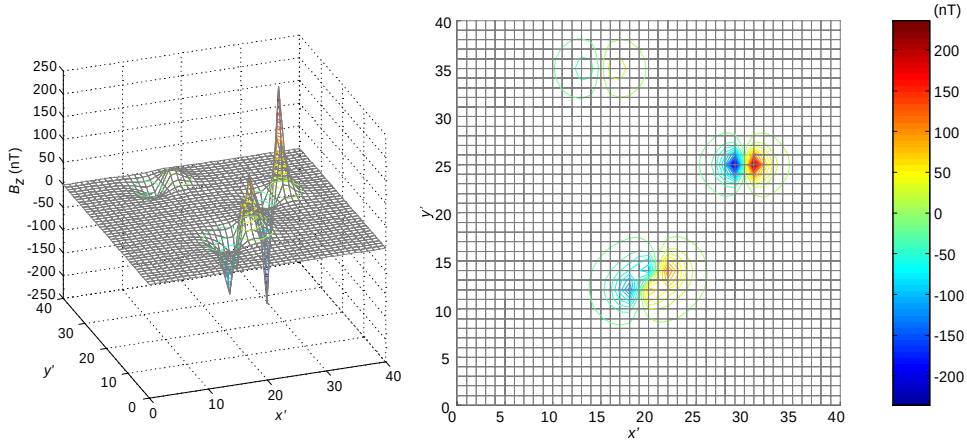

Fig.9 2-D distribution of B_z (CASE1).

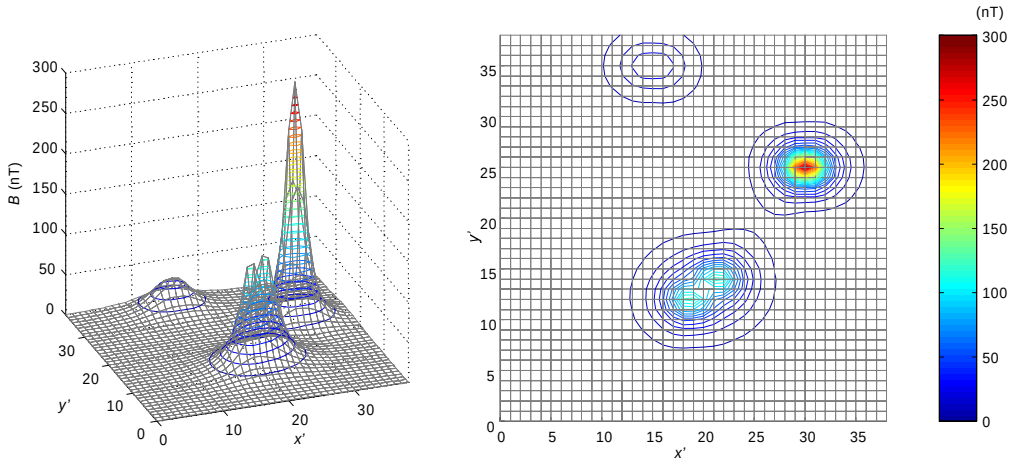

Fig.10 2-D distribution of B (CASE1).

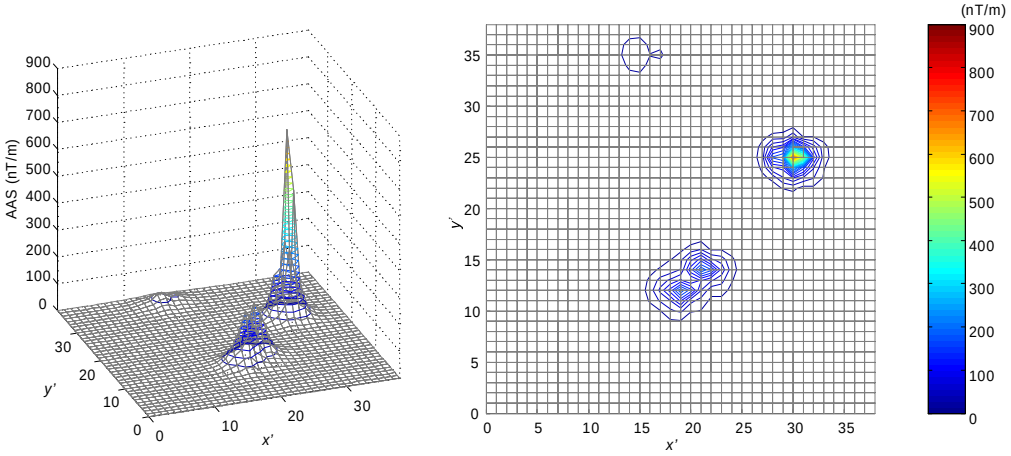

Fig.11 2-D distribution of AAS (CASE1).

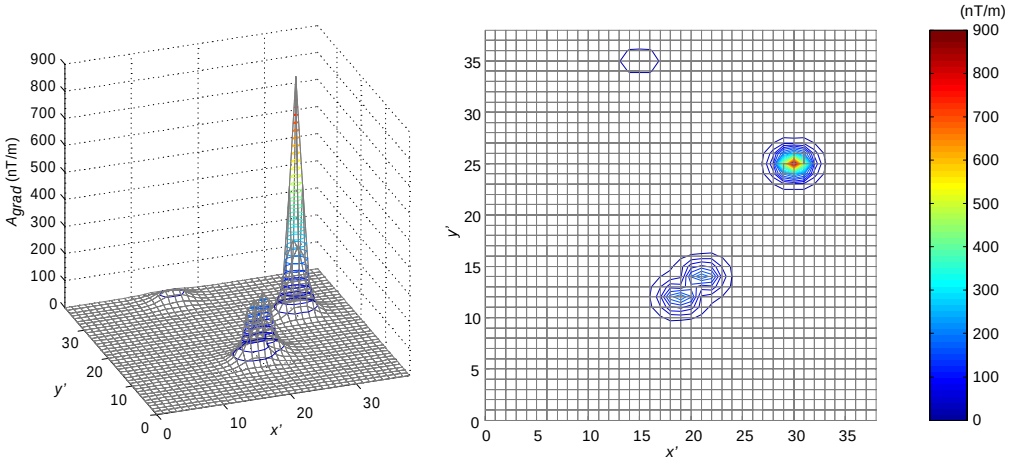

Fig.12 2-D distribution of A_{grad} (CASE1).

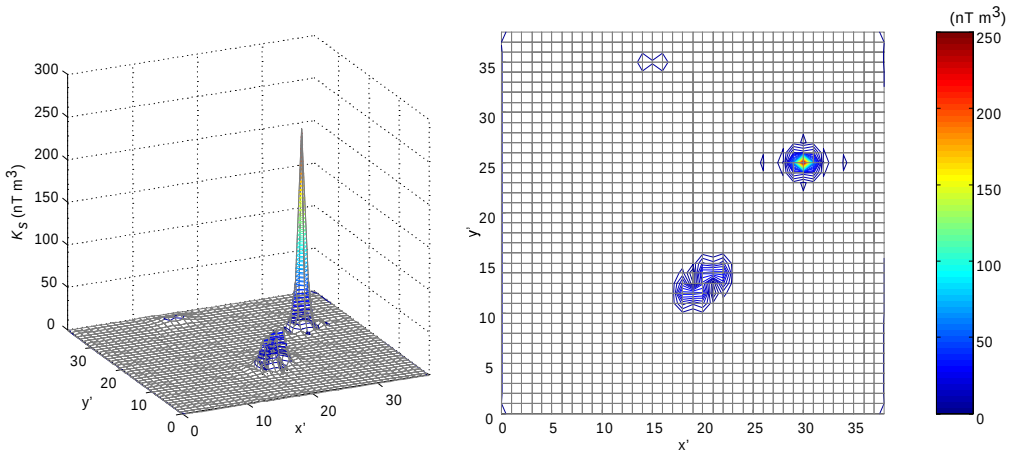

Fig.13 2-D distribution of K_s (CASE1).

Table 3 Simulation Model (CASE2).

Positions of Magnetic Sources	(x, y, z) = (3.0 2.0 -1.0), (7.0 8.0 -1.5), (6.0 4.0 -0.5)
Amplitude of Uniform Magnetization*1	1000 [A/m]
Size of Magnetic Sources*1	A right cylinder with 0.2 m diameter and 0.1m height
Inclination and Declination Angles of Geomagnetic Field	$a_g = 47^\circ 38^{''}$, $\beta_g = 6^\circ 35^{''}$
Size of Observation Field	10 [m] × 10 [m]
Height of Observation	$z_o = 1.0$ [m]
Number of Grid Points for Observation*2	$N_o = 40 \times 40$ [points]
Number of Grid Points for Magnetic Source Estimation*2	$N_s = 10 \times 10$ [points]
Mean and Variance of Observation Noises	(mean) = 0.0 [m], (variance) = 100.0 [m^2]

*1 for all the anomalies, *2 uniformly distributed in the observation field.

On the other hand, the distribution of the estimated K_s shows the exact magnetic sources as well as other apparent anomaly sources caused by the estimation errors as shown in **Fig.17**.

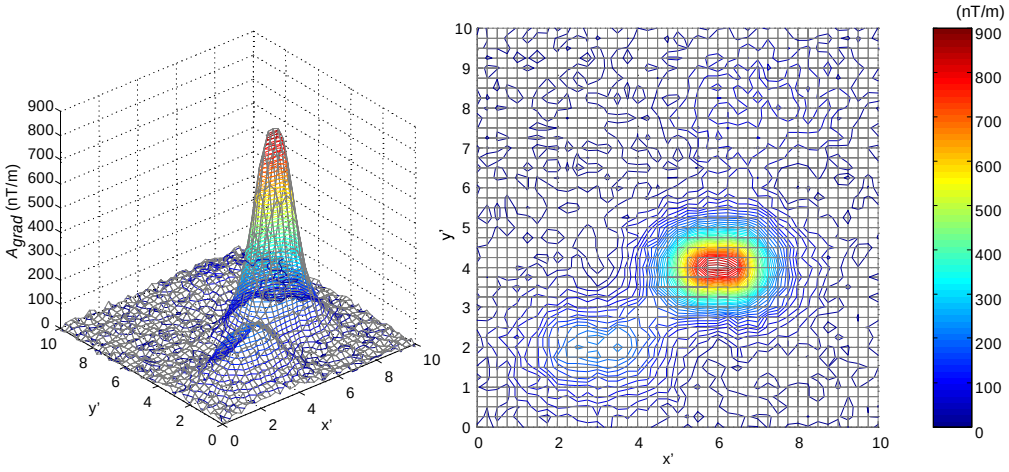

Fig.14 2-D distribution of A_{grad} (CASE2).

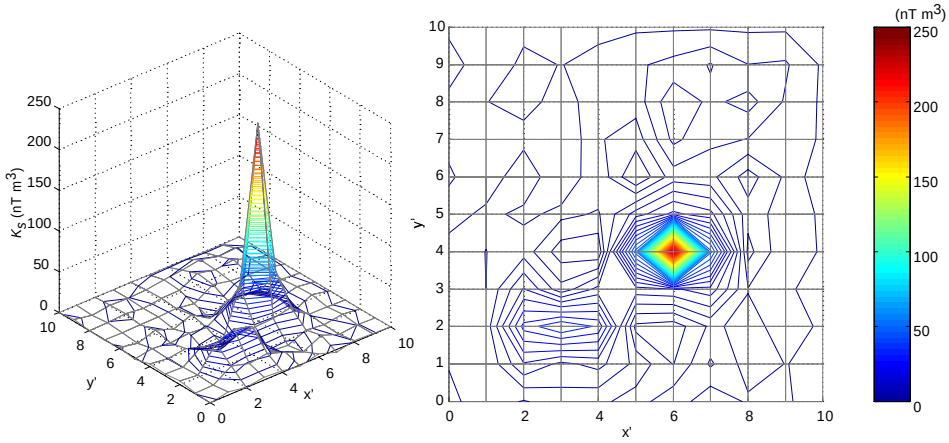

Fig.15 2-D distribution of K_s (CASE2).

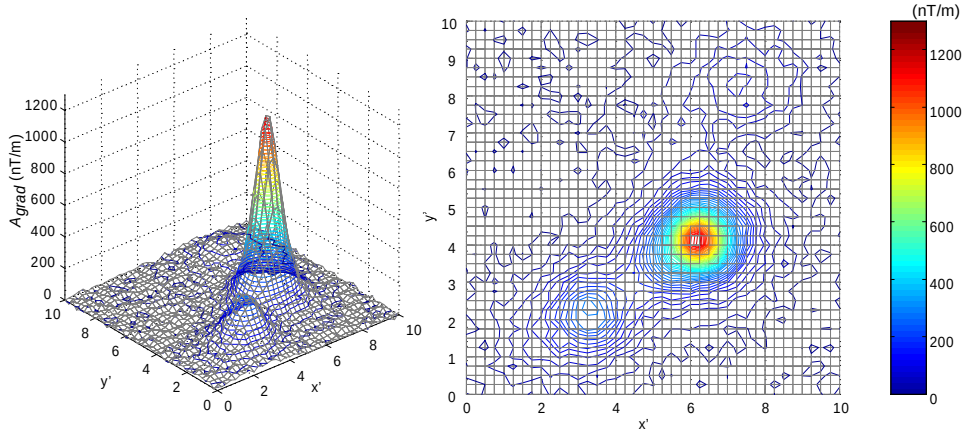

Fig.16 2-D distribution of A_{grad} (CASE2, for the case that $\alpha = \pi / 6.0$ [rad] and $\beta = \pi / 6.0$ [rad]).

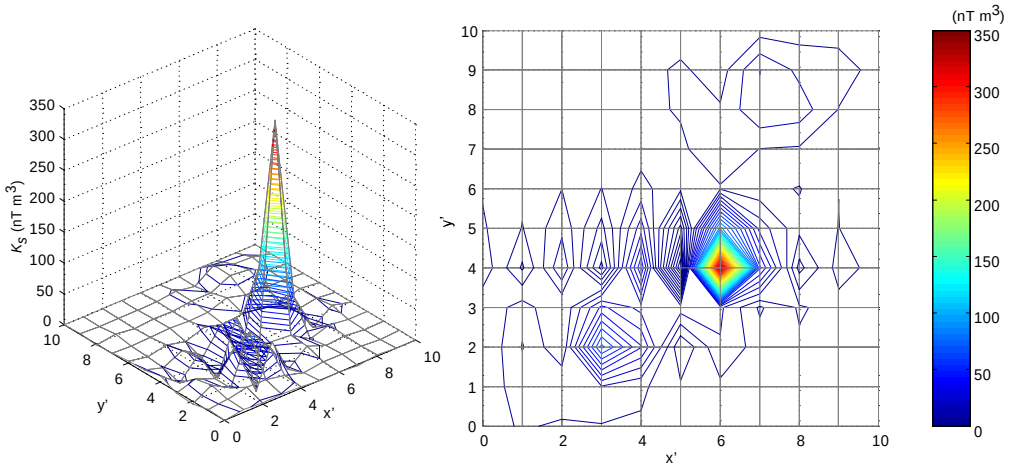

Fig.17 2-D distribution of K_s (CASE2, with estimation error of the magnetization directions).

4.3 Indoor experiment

An indoor experiment has also been conducted to validate the proposed method. The magnetic gradiometer used in this experiment and the specifications of the sensor are shown in **Fig.18** and **Table 4**, respectively. As shown in **Fig.18**, two magnetic sensors are mounted on each end of the sensor unit at a distance of 0.5 [m]. Outputs of this sensor through the signal processing unit are magnetic inductions in three different directions observed at each end, $B_{x_1}, B_{x_2}, B_{x_3}, B_{y_1}, B_{y_2}, B_{y_3}$, as well as the variations of the inductions between two sensors in each direction, $\Delta B_x, \Delta B_y, \Delta B_z$.

In this experiment, as a test piece simulating an anti-tank mine, a cylindrical iron (diameter;6.9 [cm], height;3.3 [cm]) is used. Although ferromagnetic material included in this can is about 0.24 [kg], an anti-tank mine normally includes greater than 0.4 [kg]. Therefore, if this test piece is detected during the experiment, real anti-tank mines may be more easily detected by using the proposed method.

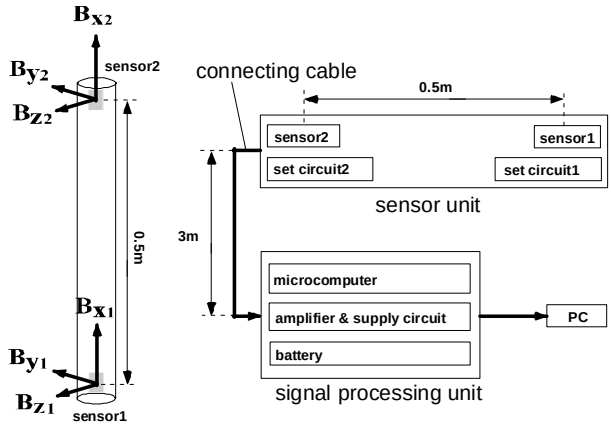

(a) sensor unit (b) system components

Fig.18 The magnetic gradiometer used in the experiment.

Table 4 Specifications of the magnetic gradiometer.

Magnetic Sensor	HMC2003 (Honeywell Co.)
Accuracy	4 [nT]
Dissipation Power	Max. 0.3 [W]
Operating Temperature	-40 °*C* to 85 °*C*
Range	± 200000 [nT]
Size	Triangle pole (cross-section 4.5 [cm^2], height 65 [cm])
Weight	300 [g]

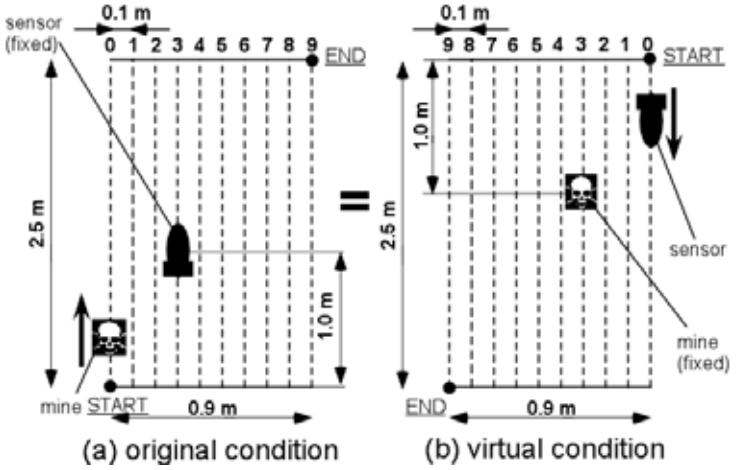

Fig.19 Relationship between the original and the virtual condition for the experiment.

As shown in **Fig.19 (a)**, a test field with the size of 2.5×0.9 [m] is divided by nine parallel lines at a distance of 0.1 [m] and the test piece moves along each line at a constant velocity from one end to the other, in the order of numbers. The magnetic gradiometer is fixed at (0.3, 1.0) [m] from the starting point, and at an altitude of 0.75 [m] above the ground. The sensor obtains data at a constant sampling rate. This experimental condition virtually simulates the one as shown in **Fig.19 (b)**, where the mine is fixed on the ground but the sensor moves along parallel lines over the test field.

Figure 20 shows some of the results of $\Delta B_x, \Delta B_y, \Delta B_z$ observed along the line No.3 in **Fig.19 (a)**. Also, **Figs.21** to **24** show the 2-D distributions of AAS and estimated K_s.

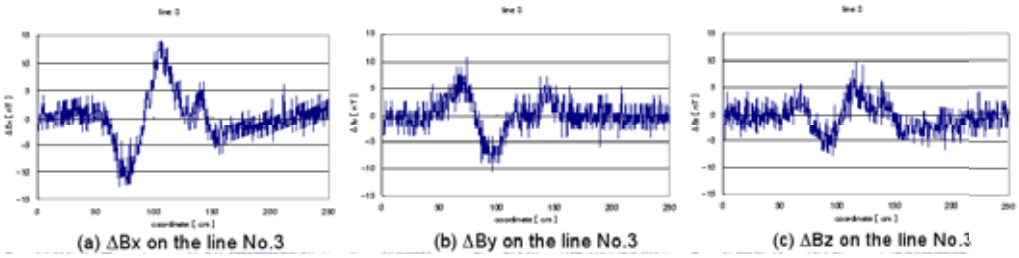

Fig.20 Results of the observed data during the experiment.

Table 5 Comparison between two methods to detect an anomaly source.

	AAS	Proposed method
Estimated position [m]	(0.22, 0.99)	(0.23, 1.0)
Error [m]	0.079	0.074

Though the difference between two methods is hard to be seen only from these figures, the effectiveness of the proposed method is shown in **Table 5** as the value of the estimation error. In this experiment, the distance between the sensor and the magnetic source is relatively short and the effect to remove the observation noise is not clear. Various cases with respect to the depth of a magnetic source should be considered in future experiments.

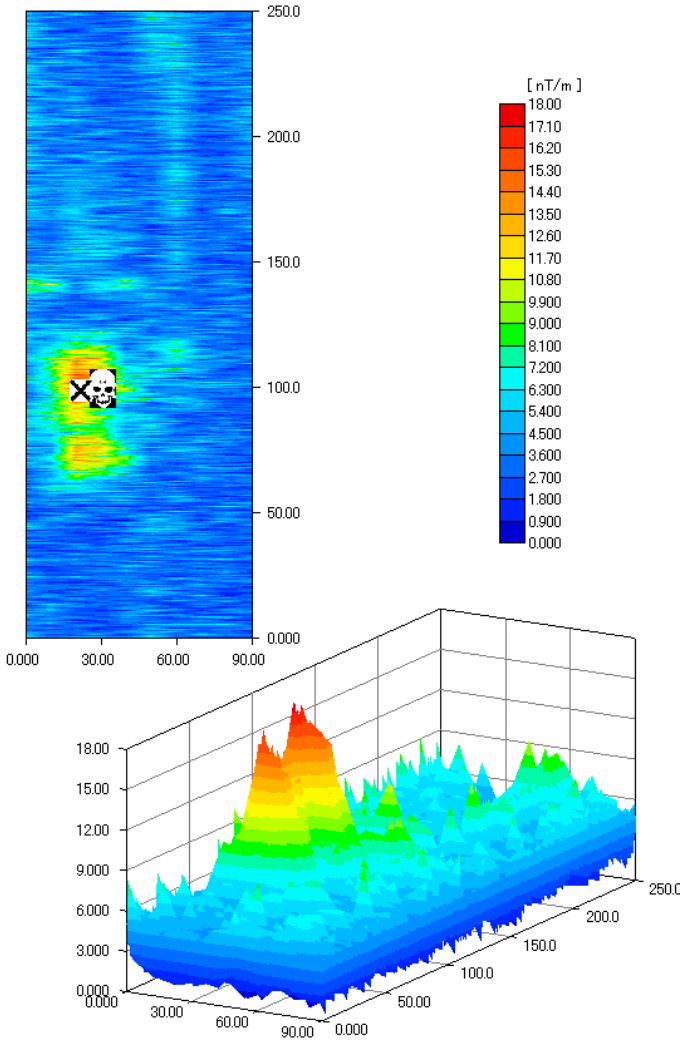

Fig.21 2-D distribution of AAS for the experimental data.

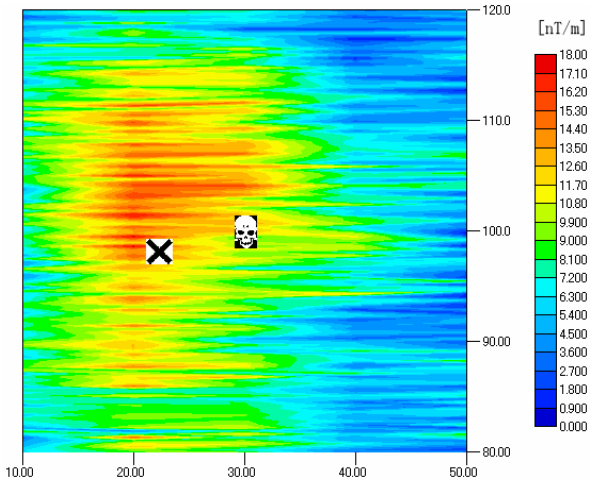

Fig.22 2-D distribution of AAS for the experimental data (around magnetic source).

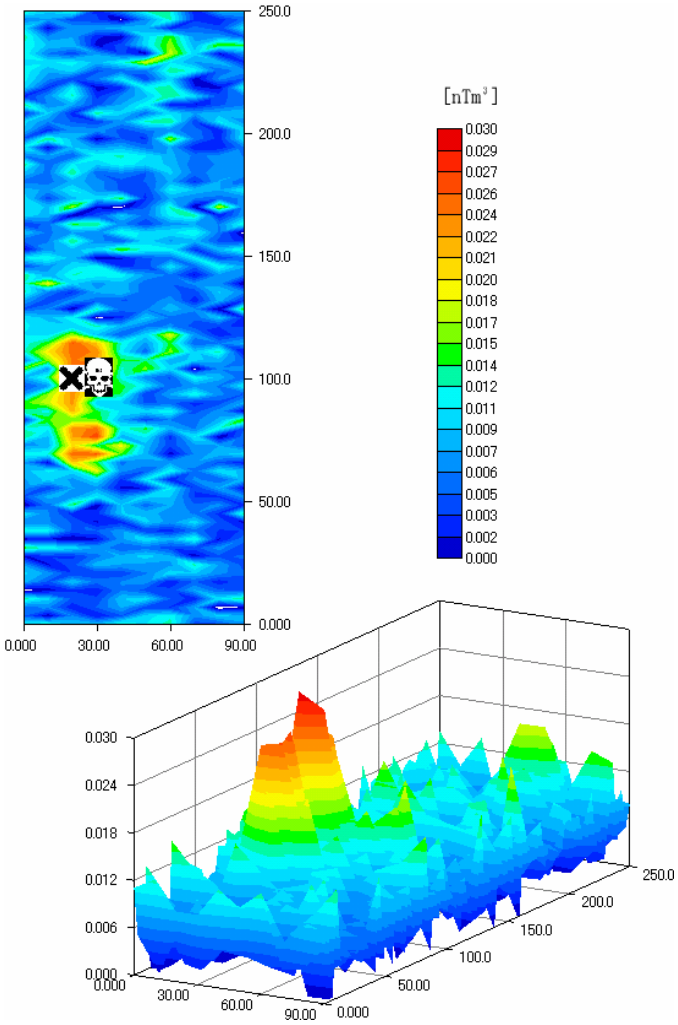

Fig.23 2-D distribution of the estimated parameter of the magnetic dipole.

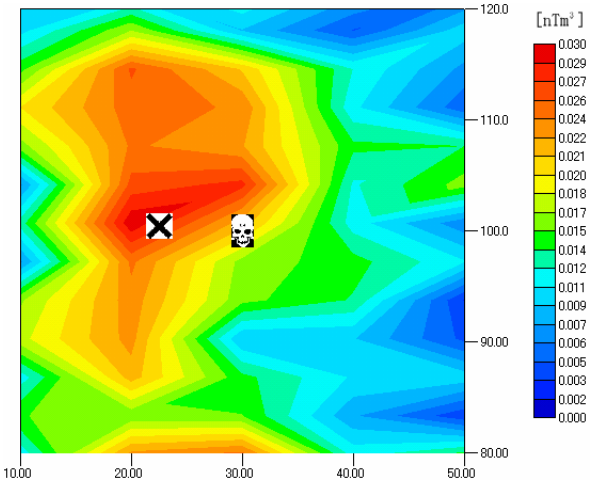

Fig.24 2-D distribution of the estimated parameter of the magnetic dipole. (around magnetic source)

5. Improvement of the Proposed Method

According to the results of numerical simulations, the effectiveness of the proposed method has not been necessarily validated for the case where the assumption about the magnetization direction of magnetic sources at each grid point is too rude. In this section, another method to improve the estimation error of the magnitude of magnetic induction at each grid point is proposed.

As previously mentioned, the parameter concerned with the magnitude of magnetic induction of a dipole buried at a grid point, $\mathbf{K_s}$ is estimated by Eq. (17). However, some of the components of $\mathbf{K_s}$, $\delta_1, \delta_2, \delta_3, \cdots, \delta_{k_1}$ are so small that they are negligible because of the distances sufficiently far from the positions of real magnetic dipoles.

Therefore, at the first step (STEP1 as shown in **Fig.25**), all the components of the estimated $\mathbf{K_s}$ smaller than a threshold value, ε ($\delta_j < \varepsilon, (j = 1,2,3,\cdots,k_1)$), and their corresponding rows in the matrix $\mathbf{C}^*$ are removed. This operation means that all the grid points at which magnetic sources do not exist apparently (or far enough from an observation point) are eliminated from the computation in order to decrease estimation error as well as computational load.

At the next step (STEP2), from the shrunk $\mathbf{C}^*$ ($= \mathbf{C}^{*(1)}$) and the original $\mathbf{A_{grad}}$, new $K_s(i)$ ($= K_s{}^{(1)}(i)$, $i = 1,2,3,\cdots,N_s - k_1$) is calculated. At this step, the same procedure as at STEP1 is taken by removing all the components of the $\mathbf{K_s}^{(1)}$ smaller than ε and their corresponding rows of $\mathbf{C}^{*(1)}$. The procedure stated above is repeated until the final step (STEP *f*), which is appropriately chosen. The proposed scheme is schematically shown in **Fig.25**. To be noted here is that all the components of $\mathbf{K_s}$ which are removed ($\delta_j < \varepsilon, (j = 1,2,3,\cdots)$) during the computation are set equal to zeros when all the components of $\hat{\mathbf{K}}_{\mathbf{s}}{}^{(f)}$ are finally obtained. By using this method, 2-D distribution of $\mathbf{K_s}$ is estimated from the 2-D distribution of the original observation data $\mathbf{A_{grad}}$ in **Fig.16** as shown in **Fig.26** ($f = 2$ in this case).

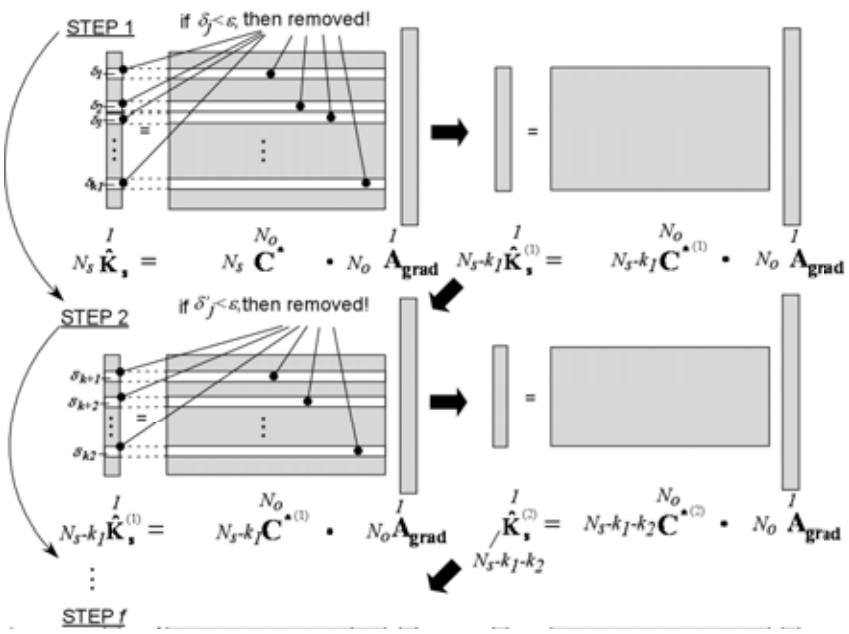

Fig.25 Improved method to estimate $\mathbf{K}_s$.

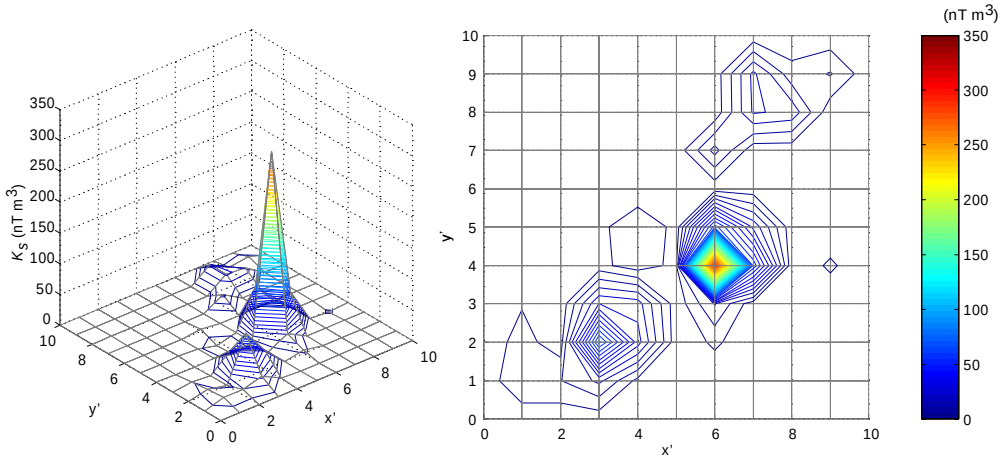

Fig.26 2-D distribution of the estimated $\mathbf{K}_s$ (CASE2, by the improved method).

Comparing this result with **Fig.17**, the estimation error is remarkably improved even in the case where the assumption on the magnetic sources' magnetization direction is rude to some extent.

6. Conclusion

In this study, a new approach to airborne mine-detection using magnetic gradiometer is proposed. As for the land mines containing much ferromagnetic material such as anti-tank mines, they can be detected as some anomalies of a dipole magnetic field. On the other hand, when such

a magnetic sensor is carried onboard an aircraft such as a blimp, observation noise caused by other onboard devices cannot be ignored.

Therefore, the method to detect the 2-D positions of magnetic anomaly sources by estimating the magnitudes of magnetic inductions buried under grid points in an observing field through the Least Squares method is proposed. Numerical simulations and an indoor experiment have validated that the proposed method is effective to focus on the regions where mines are buried as well as to extract anomaly sources hidden in noises.

More experiments changing the parameters such as the depth at which a mine is buried, and the mine's direction of magnetization should be conducted, and eventually outdoor experiments using a blimp are left as the future work.

References

1) Kyushu University mine action group (QMAG) and Center for northeast Asian studies, Tohoku University, The Evaluation Test Survey for Landmine Detection in Egypt, Report submitted to the Embassy of Arab republic of Egypt, Tokyo, Japan (2005).
2) R. J. Blakely, Potential Theory in Gravity and Magnetic Applications, Cambridge University Press, (1995).
3) W. R. Roest, J. Verhoef, and M. Pilkington, Magnetic Interpretation using 3-D Analytic Signal, Geophysics 57, pp. 116-125 (1995).